IEEE Photonics Journal
An IEEE Photonics Society Publication

A Silicon Photonic PAM-4 Modulator Based on Dual-Parallel Mach–Zehnder Interferometers

Volume 8, Number 1, February 2016

Alireza Samani
Venkat Veerasubramanian
Eslam El-Fiky
David Patel
David V. Plant

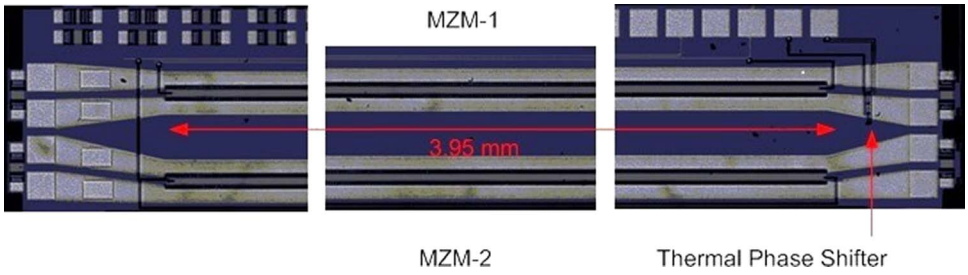

DOI: 10.1109/JPHOT.2015.2512105
1943-0655 © 2015 IEEE

A Silicon Photonic PAM-4 Modulator Based on Dual-Parallel Mach–Zehnder Interferometers

Alireza Samani, Venkat Veerasubramanian, Eslam El-Fiky, David Patel, and David V. Plant

Department of Electrical and Computer Engineering, McGill University, Montréal, QC H3A 0E9, Canada

DOI: 10.1109/JPHOT.2015.2512105

Manuscript received December 8, 2015; accepted December 19, 2015. Date of publication December 29, 2015; date of current version January 11, 2016. This work was supported in part by the Silicon Photonic Electrically Engineered Devices (SPEED) research project, funded by the Natural Sciences and Engineering Research Council of Canada (NSERC) (RDCPJ438811-12), PROMPT (PJT-2011-17), and TeraXion; by the contribution and technical support of CMC Microsystems; and by NSERC under SiEPIC CREATE. Corresponding author: A. Samani (e-mail: alireza.samani@mail.mcgill.ca).

Abstract: We present a silicon photonic dual-parallel Mach–Zehnder modulator (MZM) operating near 1550 nm used for four-level pulse amplitude modulation (PAM-4). The differential and integral nonlinearities of the device are investigated. A driving scheme and a biasing method that improves the linearity and PAM operation of the device are presented. The measured second harmonic distortion and two-tone, third-order intermodulation spurious-free dynamic range are 75 dB $\cdot$ Hz$^{1/2}$ and 86 dB $\cdot$ Hz$^{3/2}$, respectively. We further investigate the performance of the device in a short-reach transmission system. We report a successful 50-Gbaud single-wavelength transmission of PAM-4 over 2 km of single-mode fiber (SMF) below hard decision pre forward error correction (pre-FEC) threshold of 4.4×10^{-3}.

Index Terms: Silicon nanophotonics, electro-optical systems, microwave photonics signal processing.

1. Introduction

The demand for higher bandwidth fueled by cloud computing and web-based media applications has rapidly grown over the past few years. As a result, the need for faster and inexpensive short reach optical interconnects has become eminent [1]. The short reach interconnects employed at data centers are very sensitive to cost and footprint. Silicon photonics is an emerging technology of choice for low cost and low power optical links. The current short reach systems employ on-off keying (OOK) modulation as a cost-effective solution. However, considering the EO bandwidth requirements, OOK will not be a feasible modulation scheme for next generation optical systems operating at 100 Gb/s per wavelength. Coherent modulation schemes such as quadrature phase shift keying (QPSK) and quadrature amplitude modulation (N-QAM) offer higher spectral efficiency compared to OOK and are currently used in long haul transmission systems. However, they are not considered an attractive solution for short reach communication systems due to their receiver complexity and cost. An alternative modulation scheme which has recently gained interest in optical communications is the 4-level

pulse amplitude modulation (PAM-4) [2]. PAM-4 can achieve up to twice the spectral efficiency of OOK while using the same intensity modulation direct detection (IM-DD) receiver architecture.

PAM-4 signaling was first shown using silicon photonic (SiP) travelling wave Mach Zehnder modulator (MZM) using conventional driving circuitry [3]. However to achieve higher baud rates a more complex optical and electrical designs were required. There have been two general approaches to optical PAM-4 generation. First, producing PAM-4 optical signals by driving a MZM or vertical-cavity surface-emitting lasers (VCSEL) using a digital-to-analog converter (DAC) and digital-signal-processing (DSP) [4]–[8]. More recently electro-absorption modulators (EAM) driven by DAC were successfully used to transmit PAM-4 signals without using DSP [9]. Secondly, using bit pattern generators (BPG) or conventional drivers to drive multi-electrode MZM (ME-MZM) [10], [11] which eliminates the need for a DAC, an analog-to-digital convertor (ADC), and DSP resulting in relatively lower power consumption and cost. Silicon photonic modulators with high bandwidth, relatively low drive voltages and compatibility with complementary metal-oxide-semiconductor (CMOS) process have shown to be capable candidates for both methods [4], [10]. As the next generation 400 GE systems are being developed and there are no standard methods for generating PAM-4, it is very important to explore different architectures, driving schemes, and platforms to identify an efficient PAM modulator.

In this paper we present an alternative silicon photonic PAM modulator based on dual parallel MZMs (DP-MZM). To the best of our knowledge, this is the first time that PAM-4 transmission is shown using a silicon photonic DP-MZM. We present and experimentally validate a driving and biasing method to increase the linearity of the DP-MZM to produce four equally spaced PAM-4 levels using two independent driving signals. The presented driving scheme can be further applied to commercially available DP-MZMs to achieve PAM-4 modulation. Similar to ME-MZM, the dual parallel architecture can be used to generate PAM-4 signals without the use of ADC/DAC and DSP. In the absence of DSP, the PAM-4 signal can be directly detected by PD+TIA and assigned a value corresponding to the two bit combination using an electrical encoder consisting of flip flops and combiners [12]. Differential and integral non-linearities of the device are investigated to ensure that equidistant power levels are achieved. The measured second harmonic distortion (SHD) and two tone third order intermodulation (IMD3) spurious free dynamic range (SFDR) are 77 dB.Hz$^{1/2}$ and 81 db.Hz$^{3/2}$, respectively. We operate the device at 50 Gbaud PAM-4 on a single wavelength. We characterize the chirp parameter of the device under various bias voltages. The measured –0.5 chirp parameter counteracts the dispersion of SMF-28e+ at C-band. An estimated pre forward error correction (pre-FEC) bit error rate (BER) below the hard decision FEC threshold of 4.4×10^{-3} is achieved after propagation through 2 km of SMF-28e+ fiber.

2. Device Design, Fabrication and PAM-4 Operation

The DP-MZM was fabricated in a multi project wafer run at IME A*STAR on a silicon on insulator wafer with a 220 nm thick silicon layer and a 2 μm buried oxide layer. Each inner MZM have series push pull (SPP) configuration based on our previous work in [4] and are designed to operate in the C-band. The SPP configuration of the MZM lowers the microwave losses and improves modulation bandwidth compared to the conventional dual differential drive scheme. In addition it requires only one driving signal which simplifies the operation of the device [13], [14]. All the design parameters, such as doping densities, PN junction geometries, electrode length, and geometry, were identical to [4] except the active phase shifter length of each MZM which was changed to 3.95 mm to accommodate the extra optical routing in the dual parallel design. Relative to [4], the phase shifter length reduction results in slightly higher V_π and lower optical insertion loss. Fig. 1 demonstrates the layout of the DP-MZM. DP-MZM consists of two SPP-MZMs connected in parallel to each other. Balanced 3-dB Y-branches are used at the input and output of the DP-MZM to divide and combine the light going in and out of each branch. The insertion loss of each Y-branch is measured to be 0.3 dB. The outer MZI of the DP-MZM is designed to have balanced branch lengths, to ensure that the OOK modulated outputs of MZI-1 and 2 are in-phase at the

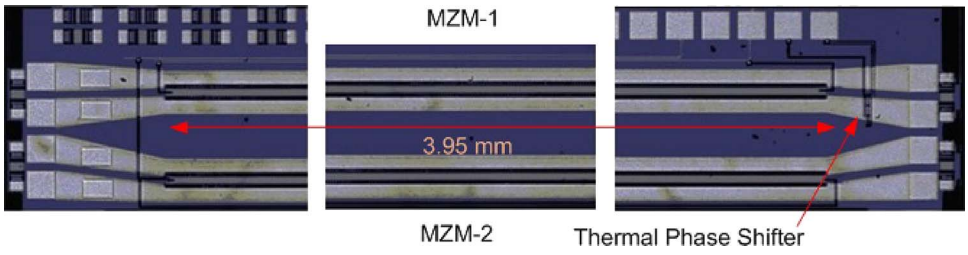

Fig. 1. Micrograph of the DP-MZM.

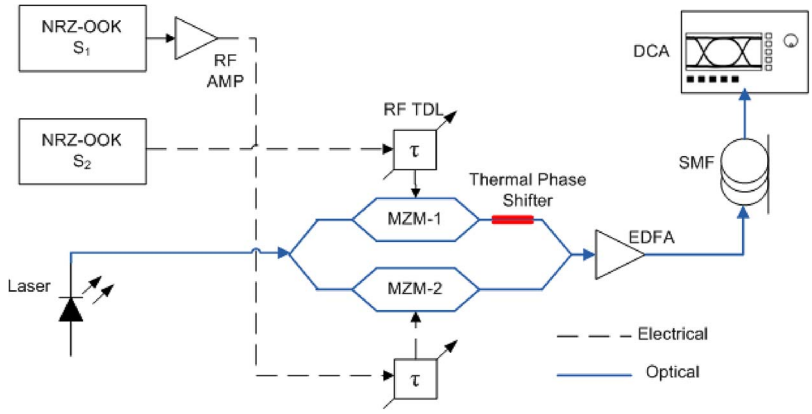

Fig. 2. PAM-4 modulation setup. (RF TDL: RF tunable delay lines.)

Y branch of the DP-MZM. To further correct the phase difference between the two branches caused by fabrication inaccuracies a thermo-optic phase shifter is placed after the output of MZM-1. Ideally, due to their push-pull operation, SPP-MZMs are expected to have no phase modulation at their output. However in case of a doping imbalance in the phase shifter between the arms of the SPP-MZM, there will be phase modulation. If the phase modulation is negligible relative to the amplitude modulation, the DP-MZM can be operated to achieve PAM-4. However, if the phase modulation is significant when the outputs of inner MZMs are combined at the outer MZM the phase modulation can result in an out of phase combination of the two signals [15]. To evaluate the phase modulation of each inner MZM, their chirp parameter is measured and presented in Section 3.3.

Fig. 2 illustrates the setup required to generate PAM-4 signals using the DP-MZM. Two independent NRZ-OOK signals; S_1 and S_2 are generated using a pulse pattern generator (PPG) with the maximum baud rate of 50 Gbaud. S_1 is then amplified by 6 dB in respect to S_2, such that S_1 and S_2 represent the most significant bit (MSB) and the least significant bit (LSB), respectively. Two tunable RF delay lines are used to accurately align the transitions of each bit stream. S_1 and S_2 are applied to MZM-1 and MZM-2, respectively. MZM-1 and MZM-2 are independently biased such that the 0 power level of each MZM corresponds to the same optical power level.

3. Device Characterization and Performance

Due to higher number of power levels in PAM-4 modulation format the non-linearity of the PAM modulator plays a significant role in achieving equidistant power levels and higher baud rates. As the PAM-4 modulation gains more attention, it is crucial to have a universal benchmark for evaluating the linearity performance of PAM modulators. Differential non-linearity (DNL) and integral non-linearity (INL) are the two measures of linearity commonly presented for a DAC. The same methodology can be applied to the presented DP-MZM to evaluate the linearity of the device as a 2-bit optical DAC. In addition, at higher baud rates the effects of intermodulation distortion and

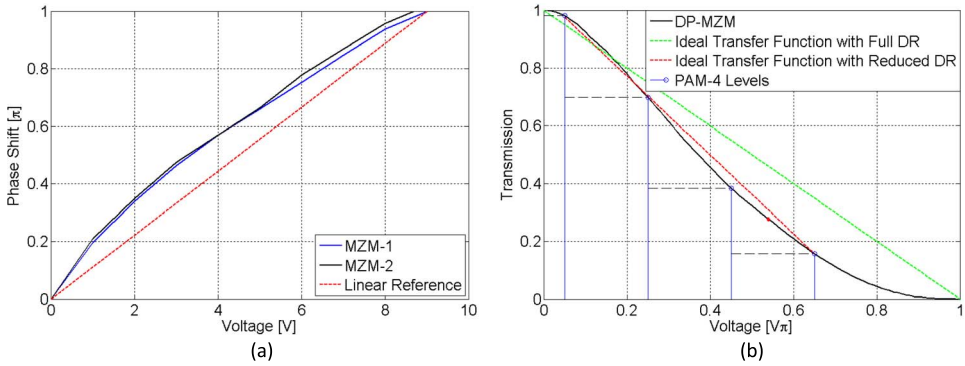

Fig. 3. (a) Phase shifter versus voltage applied to each MZM. (b) DP-MZM transfer function with both inner MZMs at the same bias voltages. Green dotted line presents an ideal linear transfer function of DAC with full drive voltage range, and the red dotted line presents the idea linear transfer function with reduced drive voltage swing.

compression result in degradation of the modulated signal as observed in the eye diagram and BER measurements presented in Section 4. Microwave linearity of optical modulators such as Spurious Free Dynamic Range (SFDR) and third-order intermodulation distortion (IMD3) can be used to evaluate the performance of optical modulators at higher baud rates.

3.1. Measurement of Linearity

In this section we present the linearity performance of the DP-MZI to evaluate its potential compared to other previously presented SiP PAM modulators.

The $V_\pi L_\pi$ of each inner MZM was measured separately using the same method presented in [5]. To measure the phase shift versus voltage for each inner MZM, various voltages were applied across the diode on one arm of the inner SPP-MZM while the diode on the other arm of the SPP-MZM was shorted to have 0 phase shift. The measured phase shift of each arm under different voltages was used to construct Fig. 3(a). As expected the two parallel inner MZMs exhibit very similar $V_\pi L_\pi$ performance of 3.55 and 3.47 V-cm, which agrees with our single MZI characteristic presented in [4]. The transmission curve of the DP-MZM with the assumption that the Y-branches have 50/50 splitting ratio and the same voltage is applied to both MZMs is shown in Fig. 3(b). Fig. 3(b) illustrates the transfer function of DP-MZM using the measured phase shift [16].

INL is defined as the maximum deviation of the DAC's analog output (transfer function) from an ideal linear fitted line in terms of the least significant bit (LSB), and can be calculated as [17]

$$\mathrm{INL} = \left(\frac{V_B - V_{\mathrm{zero}}}{V_{\mathrm{LSB}}}\right) - B \tag{1}$$

where V_B is the analog output corresponding to the digital binary input B, and V_{LSB} is the ideal spacing between two adjacent analog outputs. In an ideal DAC, all intensity steps equal V_{LSB} and the INL will be 0. Differential non-linearity is used to quantify DAC's output precision and is defined as the difference between an actual step height and the ideal value of LSB [17]

$$\mathrm{DNL} = \left(\frac{V_B - V_{B-1}}{V_{\mathrm{LSB}}}\right) - 1. \tag{2}$$

As shown in Fig. 3(b), due to the inherent non-linear transmission function of MZMs, achieving equidistant power levels of PAM-4 signal is quite challenging. When DP-MZM is operated at its full drive voltage dynamic range (DR), the INL and DNL are estimated to be 0.58 and 0.33 LSB, which result in very uneven PAM-4 intensity level distribution. The green dotted line in Fig. 3(b) represents the ideal linear transfer function of a DAC. Therefore, some linearization techniques are required to further improve the operation of PAM-4 modulator. To improve the linearity of a

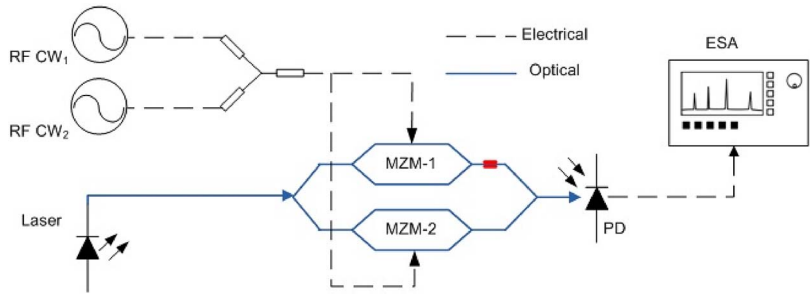

Fig. 4. SFDR measurement setup.

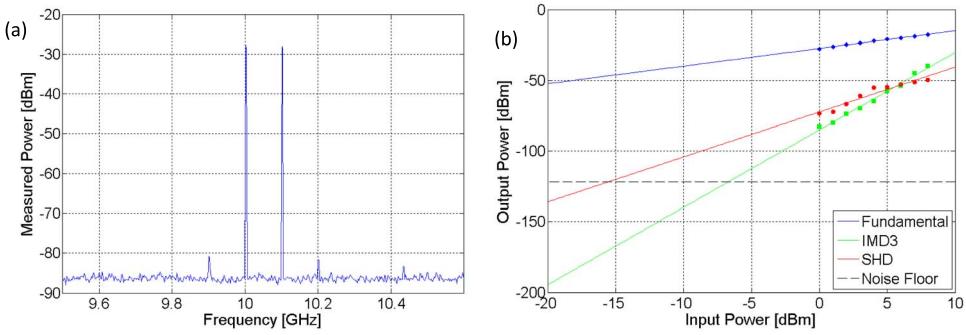

Fig. 5. (a) Measured RF spectrum of the DP-MZM for 0 dBm input power. (b) Output power versus input power of second harmonic distortion and third intermodulation distortion, with measured spurious-free dynamic ranges of −75 dB Hz $^{1/2}$ and −86 dB Hz$^{3/2}$ for $SFDR_{SHD}$ and $SFDR_{IMD3}$, respectively.

DP-MZM and mitigate the effects of its nonlinear transfer function, we reduce the operating drive voltage DR of the device to 0.63 V_π, which corresponds to 6 $V_{p\text{-}p}$ by restricting the drive voltages of MZM-1 and MZM-2 to 0.42 V_π and 0.21 V_π (4 $V_{p\text{-}p}$ and 2 $V_{p\text{-}p}$ respectively), and biasing each MZM such that the 0 levels of both MZMs correspond to a same optical output power. The corresponding bias voltages for MZM-1 and MZM-2 are 4 V and 5 V, respectively, for which the resulting INL and DNL are calculated to be 0.21 and 0.11 LSB, respectively. The red dotted line represents the ideal linear transfer function of a DAC with reduced drive voltage dynamic range. A lower drive voltage dynamic range would result in a better linearity performance of the device; however it will also decrease the height of each step, which in practice result in lower extinction ratios, and ultimately degrades the bit error rate performance. It should be noted that the 0.63 V_π drive voltage swing was measured empirically. The reduction in drive voltage swing is dependent on the phase shifter's $V_\pi L_\pi$ value and can vary with doping densities. However, the biasing and driving scheme presented to achieve four equally spaced levels can be applied to any DP-MZM.

3.2. Spurious Free Dynamic Range

We further examine the SHD and IMD3 SFDR performance of the DP-MZM. Fig. 4 demonstrates the SFDR measurement setup. A 14 dBm TE polarized light from a high power tunable laser is coupled into the DP-MZM and the output light is then amplified to 3 dBm using an erbium doped fiber amplifier (EDFA). A 35 GHz photodetector followed by a 40 GHz RF spectrum analyzer is used to detect the signal. Two RF sources are combined and then applied to the DP-MZM using 40 GHz RF probes.

Fig. 5(a), shows a RF spectrum for two tone IMD3 of the DP-MZM. The RF input signals are centered at 10.05 GHz with 100 MHz spacing. From the measurement resolution bandwidth of 4 kHz, the noise power density is calculated to be −122 dBm/Hz and is used to obtain SFDR.

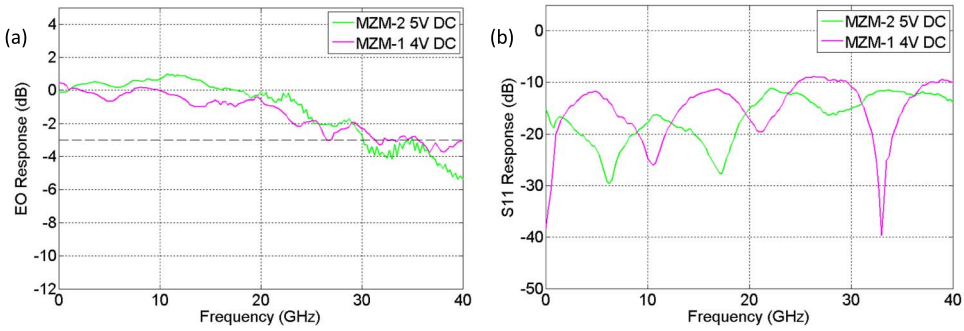

Fig. 6. (a) EO S21 response of MZM-1 and MZM-2, with measured 3 dB bandwidth of 27 and 30 GHz for MZM-1 and MZM-2, respectively. (b) S11 response of MZM-1 and MZM-2.

Fig. 5(b) illustrates the second and third harmonic SFDR of the device for different input signal powers. The amplified spontaneous emission (ASE) noise of the EDFA can cause a slight increase in the noise floor and can be lowered by sending the output through an optical filter or lowering the optical losses due to on-chip routing hence eliminating the need for the EDFA [18]. The $SFDR_{SHD}$ and $SFDR_{IMD3}$ at PAM operating DC bias voltages are measured to be 75 $dBm/Hz^{1/2}$ and 86 $dBm/Hz^{3/2}$ which are similar to reported values for $LiNbO_3$ and SiP modulators [19], [20]. This indicates that the second and third harmonics are suppressed sufficiently and that the SFDR of the device is more than adequate to prevent intermodulation distortion. These values can be further improved by adjusting the power splitting ratio at the outer MZM, as shown in [16].

3.3. Small Signal and Chirp Measurements

To evaluate the modulation efficiency of the DP-MZM, we examine the small signal electro-optic response of each of the MZMs separately. Two high frequency RF probe with a GSSG configuration are used to drive the transmission line of each MZM at one side and to terminate the line with 50 Ω at the opposite end. A 50 GHz lightwave component analyzer (LCA) is used to characterize the small signal properties of MZM-1 and 2 at 4 V and 5 V DC bias voltages used for PAM operation as described in Section 3. Fig. 6(a) curves are normalized to the response at a reference frequency of 1.5 GHz. The observed bandwidth of each MZM is lower than the measured values in [4] which could be due to different tapering of the electrodes and difference in transitions between the PN-junction loaded and unloaded sections compared to [4]. Nevertheless, the observed 31.5 and 30 GHz bandwidths at operating conditions of MZM-1 and MZM-2 have been shown to be sufficient for 50 Gbaud OOK transmissions [13]. The S11 responses of both modulators shown in Fig. 6(b) indicate that the reflection caused by impedance mismatch is sufficiently low and a good impedance matching is achieved.

Since the device is designed to operate close to 1550 nm, fiber dispersion plays a significant role in quality of signal transmission through fiber. To evaluate the susceptibility of the DP-MZM to dispersion, we investigate the small signal chirp parameter of the device, by measuring its EO response after propagating through a 36 km long dispersive SMF-28 fiber. The dispersion of the SMF-28 fiber and the modulator chirp can be found from resonance frequencies [21]. Fig. 7(a) shows the corresponding EO response of the link when both MZMs are biased at their PAM-4 operating DC voltages. The relationship between the resonance dips of the EO response and the chirp and dispersion parameter of the system are given by [21]

$$f_u^2 L = \frac{c_0}{2D\lambda^2}\left(1 + 2u - \frac{2}{\pi}\arctan(\alpha)\right) \tag{3}$$

where f_u is the uth order resonance dip of the EO response, c is the speed of light, D is the dispersion parameter of the fiber, λ is the operating wavelength, and α is the chirp parameter. Using linear regression; $f_u^2 L$ verses $2u$ is plotted in Fig. 7(b). The slope and position of the line yield the

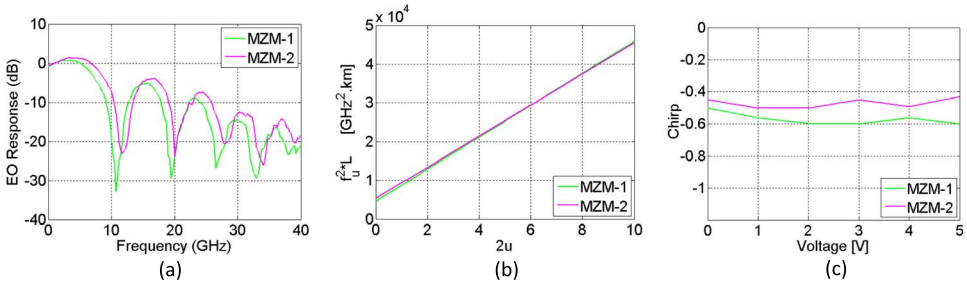

Fig. 7. (a) EO response of MZMs after 36 km of SMF. (b) Linear regression of product of measured resonance frequency and length. (c) Measured chirp of MZM-1 and MZM-2.

dispersion and chirp parameter. At the operating biases mentioned previously, both MZM-1 and MZM-2 have very similar chirp parameters of –0.58 and –0.62. We repeat the EO measurements of each MZM under different bias voltages and their corresponding chirp value is presented in Fig. 7(c). It is observed that both MZM have very close negative chirp parameter. This negative chirp is beneficial in counteracting the fiber dispersion when the output of the device is propagated through various lengths of fiber [22], [23]. In the next section, we validate this by transmitting through different lengths of single mode fiber (SMF).

4. Transmission Experiment

In this section, we examine the performance of the DP-MZM for PAM-4 transmission. The experimental setup shown in Fig. 2 is used to modulate PAM-4 signals. MZM-1 and MZM-2 are driven by 4 and 2 $V_{p\text{-}p}$ drive voltages. A 14 dBm tunable laser is used to couple light into the modulator. The total insertion loss of the device is measured to be 16.5 dB, which includes the grating coupler and routing losses of 8.5 and 2.4 dB, resulting in a device insertion loss of 5.6 dB. The modulated output of the device is then amplified using an EDFA and detected by a 65 GHz sampling head of the digital communication analyzer (DCA). Fig. 8 shows back to back NRZ-OOK and PAM-4 eye diagrams for 28 and 50 Gbaud and 50 Gbaud eye diagrams after 2 and 5 km. The OOK eyes presented are obtained by driving MZM-2 with a 2 V_{p-p} drive voltage (S2), which corresponds to the LSB of the PAM-4 format, while MZM-1 was biased at NULL such that its output corresponds to 0 PAM-4 power level. An error free operation up to 40 Gb/s were measured. The vertical eye closure penalties (VECP) for PAM-4 eye diagrams are noted below each eye diagram.

The eye diagrams presented in Fig 8. confirm that the biasing and RF amplitude swings of each MZM result in 4 equally spaced power levels. The BER of the transmission system is estimated by assuming Gaussian distribution of each level [24]. To have a better quantitative evaluation of the device's transmission performance, we numerically calculate the BER of the device for various PAM-4 baud rates using the method presented in [8]. The mean power and distribution of each PAM-4 level were measured from the eye diagrams after collecting enough samples and used to estimate BER. Fig. 9, demonstrates the estimated BER for different baud rates. We further propagate the modulated signal through various lengths of SMF 28 fiber. A successful 50 Gbaud transmission of PAM-4 over 2 km of SMF below pre-FEC hard decision threshold of 4.4×10^{-3} is achieved [25]. Considering the 7% over head of the FEC, the transmitted payload is 46.5 Gbaud. The measured negative chirp of the device is beneficial in eliminating the effects of SMF dispersion.

As presented in Figs. 8 and 9, the SiP DP-MZM is a potential candidate for PAM-4 modulation. The electrical driving circuitry components used for the DP-MZM are identical to those used for the ME-MZM presented in [10]. Both architectures have shown to be potential candidates for PAM-4 signaling up to 50 Gbaud for 2 km of reach. Both DP-MZM and ME-MZM have similar insertion loss of 16.5 dB. However, due to the longer phase shifter lengths, the DP-MZM herein presented achieves the 50 Gbaud transmission using lower drive voltages compared to [10]. It should be noted that the ME-MZM in [10] has a 2.7 dB excess insertion loss due to layout design.

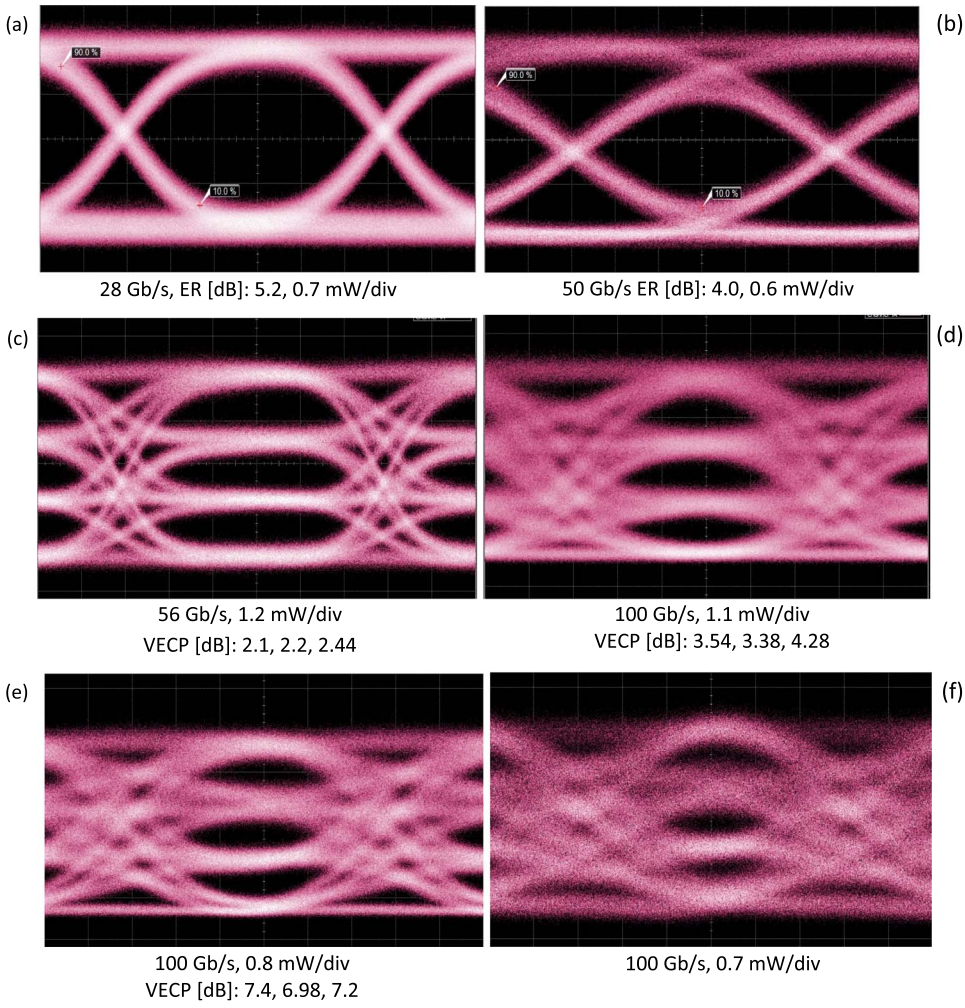

Fig. 8. Back to back (a) 28 Gbaud PAM-2, (b) 50 Gbaud PAM-2, (c) 28 Gbaud PAM-4, (d) 50 Gbaud PAM-4, (e) 50 Gbaud PAM-4 after 2 km, and (f) 50 Gbaud PAM-4 after 5 km.

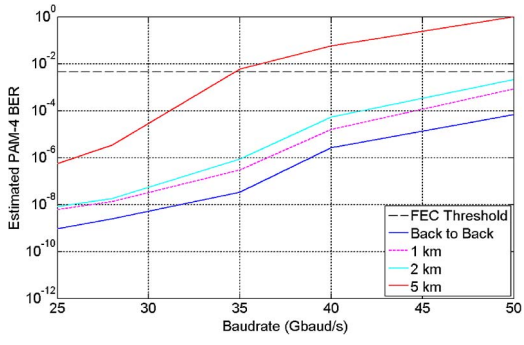

Fig. 9. Estimated BER of PAM-4 modulation versus baud rate after various fiber propagation lengths.

The DP-MZM architecture has four extra Y-branches compared to segmented electrode designs. The Y-branches used have a measured insertion loss of 0.3 dB. Assuming 4 dB insertion loss per 4 mm PN junction phase shifter, and the additional losses from the Y-branches, the estimated values of insertion loss for the DP-MZM and ME-MZMs with similar phase shifter

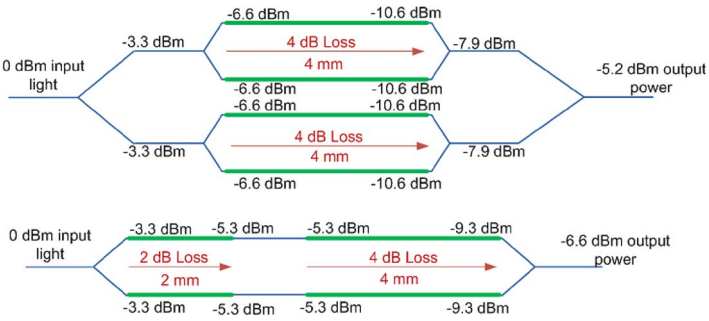

Fig. 10. Total insertion loss comparison of DP-MZM and ME-MZM.

lengths are presented in Fig. 10. As shown, the DP-MZM has 1.4 dB lower insertion loss. However the ME-MZM would require a slightly lower drive voltage to achieve a similar extinction ratio as the one obtained herein with the DP-MZM. In order to identify the optimum drive voltage/optical insertion loss tradeoff between the DP-MZM and the ME-MZM, a more detailed study of both architectures and their transfer function would be required.

5. Conclusion

In this paper, we present the design, characterization, and transmission performance of a silicon photonic dual parallel Mach Zehnder interferometer modulator capable of generating 50 Gbaud PAM-4 signal without the use of DAC and DSP. The driving method used to generate PAM-4 signals using DP-MZM is presented. The linearity of device is characterized, and it shown that by biasing each MZM independently and limiting their driving voltage, equidistant PAM-4 power levels can be obtained. The $SFDR_{SHD}$ and $SFDR_{IMD3}$ are measured to be 79 $dBm/Hz^{1/2}$ and 83 $dBm/Hz^{3/2}$. The measured negative chirp of the DP-MZM counteract the effects of dispersion, and we achieve a pre-FEC error free 100 Gb/s single wavelength PAM-4 transmission through 2 km of SMF with no DSP and dispersion compensation.

Acknowledgment

We also thank M. Chagnon for his valuable suggestions.

References

[1] G. Ghione, *Semiconductor Devices for High-Speed Optoelectronics*. Cambridge, U.K.: Cambridge Univ. Press, 2009.
[2] *IEEE Std. 802.3ba Media Access Control Parameters, Physical Layers, and Management Parameters for 40 Gb/s and 100 Gb/s Operation*, IEEE Std. 802.3ba-2010, Jun. 17, 2010. [Online]. Available: http://standards.ieee.org/findstds/standard/802.3ba-2010.html
[3] A. Samani *et al.*, "OOK and PAM optical modulation using a single drive push pull silicon Mach–Zehnder modulator," in *Proc. IEEE 11th Int. Conf. GFP*, Aug. 27–29, 2014, pp. 45–46.
[4] A. Samani *et al.*, "A low-voltage 35-GHz silicon photonic modulator-enabled 112-Gb/s transmission system," *IEEE Photon. J.*, vol. 7, no. 3, Jun. 2015, Art. ID 7901413.
[5] D. Patel *et al.*, "Design, analysis, and transmission system performance of a 41 GHz silicon photonic modulator," *Opt. Exp.*, vol. 23, no. 11, pp. 14 263–14 287, Jun. 2015.
[6] C. Xie *et al.*, "All-VCSEL based 100-Gb/s PDM-4PAM coherent system for applications in metro networks," presented at the Eur. Conf. Optical Commun., Cannes, France, Sep. 21–25, 2014, Paper P.4.3.
[7] J. Man, W. Chen, X. Song, and L. Zeng, "A low-cost 100GE optical transceiver module for 2 km SMF interconnect with PAM4 modulation," presented at the Opt. Fiber Commun. Conf., Mar. 9–13, 2014, Paper M2E.7.
[8] M. Chagnon *et al.*, "Experimental study of 112 Gb/s short reach transmission employing PAM formats and SiP intensity modulator at 1.3 μm," *Opt. Exp.*, vol. 22, no. 17, pp. 21 018–21 036, Aug. 2014.
[9] C. Caillaud *et al.*, "Low cost 112 Gb/s InP DFB-EAM for PAM-4 2 km transmission," presented at the Eur. Conf. Opt. Commun., Valencia, Spain, Sep. 2015, Paper PDP 1.5.
[10] D. Patel, A. Samani, V. Veerasubramanian, S. Ghosh, and D. Plant, "Silicon photonic segmented modulator-based electro-optic DAC for 100 Gb/s PAM-4 generation," *IEEE Photon. Technol. Lett.*, vol. 27, no. 23, pp. 2433–2436, Dec. 2015.

[11] M. Mazzini *et al.*, "25GBaud PAM-4 error free transmission over both single mode fiber and multimode fiber in a QSFP form factor based on silicon photonics," presented at the Opt. Fiber Commun. Conf., Los Angeles, CA, USA, 2015, Paper Th5B.3.
[12] J. Wei, J. Ingham, D. Cunningham, R. Penty, and I. White, "Performance and power dissipation comparisons between 28 Gb/s NRZ, PAM, CAP and optical OFDM systems for data communication applications," *J. Lightw. Technol.*, vol. 30, no. 20, pp. 3273–3280, Oct. 2012.
[13] M. Streshinsky *et al.*, "Low power 50 Gb/s silicon traveling wave Mach–Zehnder modulator near 1300 nm," *Opt. Exp.*, vol. 21, no. 25, pp. 30 350–30 357, Dec. 2013.
[14] P. Dong, L. Chen, and Y. Chen, "High-speed low-voltage single-drive push-pull silicon Mach–Zehnder modulators," *Opt. Exp.*, vol. 20, no. 6, pp. 6163–6169, Mar. 2012.
[15] C. Prodaniuc *et al.*, "56 Gb/s, PAM-4 transmission over 25 km, using IQ modulator and unequally spaced levels," presented at the Conf. Lasers Electro-Opt., San Jose, CA, USA, May 10–15, 2015.
[16] B. Mao, P. Yue, F. Hou, and Z. Liu, "Highly linear dual parallel Mach–Zehnder modulator incorporating MMI couplers," *J. Eur. Opt. Soc. Rapid Publ.*, vol. 10, pp. 388–396, Jan. 2015, Art. ID 15004.
[17] Y. Ehrlichman, O. Amrani, and S. Ruschin, "Improved digital-to-analog conversion using multi-electrode Mach–Zehnder interferometer," *J. Lightw. Technol.*, vol. 26, no. 21, pp. 3567–3575, Nov. 2008.
[18] L. Chen, J. Chen, J. Nagy, and R. Reano, "Highly linear ring modulator from hybrid silicon and lithium niobate," *Opt. Exp.*, vol. 23, no. 10, pp. 13 255–13 264, May 2015.
[19] B. Masella and X. Zhang, "Linearized optical single sideband Mach–Zehnder electro-optic modulator for radio over fiber systems," *Opt. Exp.*, vol. 16, no. 12, pp. 9181–9190, Jun. 2008.
[20] M. Streshinsky *et al.*, "Highly linear silicon traveling wave Mach–Zehnder carrier depletion modulator based on differential drive," *Opt. Exp.*, vol. 21, no. 3, pp. 3818–3825, Feb. 2013.
[21] F. Devaux, Y. Sorel, and J. Kerdiles, "Simple measurement of fiber dispersion and of chirp parameter of intensity modulated light emitter," *J. Lightw. Technol.*, vol. 11, no. 12, pp. 1937–1940, Dec. 1993.
[22] L. Chen, D. Po, and Y.-K. Chen, "Chirp and dispersion tolerance of a single-drive push–pull silicon modulator at 28 Gb/s," *IEEE Photon. Technol. Lett.*, vol. 24, no. 11, pp. 936–938, Jun. 2012.
[23] I. Kaminow, T. Li, and A. Willner, *Optical Fiber Telecommunications Volume VIA*. Burlington, MA, USA: Elsevier, 2013.
[24] C. Xie *et al.*, "400-Gb/s PDM-4PAM WDM system using a monolithic 2 × 4 VCSEL array and coherent detection," *J. Lightw. Technol*, vol. 33, no. 3, pp. 670–677, Feb. 2015.
[25] M. Scholten, T. Coe, and J. Dillard, "Continuously-interleaved BCH (CI-BCH) FEC delivers best in class NECG for 40G and 100 G metro applications," presented at the Nat. Fiber Opt. Eng. Conf., San Diego, CA, USA, 2010, Paper NTuB3.